Protein Engineering vol.10 no.4 pp.389–398, 1997

Computer modelling of the receptor-binding domains of VEGF and PIGF

T.P.Walsh and G.H.Grant[1]

Department of Biochemistry, University College, Belfield, Dublin 4, Republic of Ireland

[1]To whom correspondence should be addressed

Models of the platelet-derived growth factor (PDGF)-like domains of vascular endothelial growth factor (VEGF) and placenta growth factor (PIGF) were built based on their homology to PDGF. These domains contain most of the determinants for receptor binding. The sequences of these proteins exhibit limited but significant homology to that of platelet-derived growth factor (PDGF), a member of the cystine knot growth factor family. The eight cysteine residues that are involved in intra- and interchain disulphide bonds are conserved. Two high affinity receptors for VEGF have been identified, only one of which binds PIGF. The models presented here are consistent with results that show that VEGF receptor binding is mediated by charged residues in the loops. A comparison of the models suggests that the difference in receptor-binding specificity between VEGF and PIGF may be due to differences in the distribution of positively charged residues and the exposure of hydrophobic residues in the loops.

Keywords: cystine knot growth factors/homology modelling/PIGF/receptor-binding determinants/VEGF

Introduction

In the early 1970s, it was hypothesized that tumour growth depends on angiogenesis and that the inhibition of angiogenesis might be an effective approach to the treatment of solid tumours (Folkman, 1971). There is now much evidence to support this proposal. Tumours become vascularized by inducing angiogenesis in nearby blood vessels, causing them to produce capillaries that grow into and vascularize the tumour. At least 20 peptides have been shown to be directly or indirectly angiogenic but there is mounting evidence that the primary regulator of tumour angiogenesis is vascular endothelial growth factor (VEGF) (Ferrara *et al.*, 1993). VEGF was originally described in highly vascularized tumours where its expression is increased by hypoxia (Shweiki *et al.*, 1992) and was first isolated from bovine pituitary folliculostellate cells as a secreted heparin-binding protein of 46 kDa molecular weight (Ferrara and Henzel, 1989). It is a specific mitogen for endothelial cells and is a potent inducer of vascular permeability, which allows tumour cells to enter blood vessels (Ferrara and Henzel, 1989; Houck *et al.*, 1991). The growth of tumours *in vivo* can be suppressed by monoclonal antibodies raised against VEGF but these antibodies have no effect on the growth of tumour cells *in vitro* (Kim *et al.*, 1993). VEGF is overexpressed in glioblastoma cells and endothelial cells in tumours exhibit a 2–3-fold increased expression of the VEGF receptor *in vivo* (Plate *et al.*, 1992). Glioblastoma growth *in vivo* can be inhibited by transfecting endothelial cells with a dominant negative mutant of the VEGF receptor (Millauer *et al.*, 1994).

The molecular cloning of human cDNA for VEGF yielded four transcripts encoding species with insertions or deletions in the cDNA occurring at a common site (Tischer *et al.*, 1991). The four transcripts encoded a 26 amino acid hydrophobic signal sequence and had identical mature amino termini. The transcript encoding the 46 kDa form generates a 165 amino acid peptide following signal cleavage; this peptide is known as $VEGF_{165}$. The other transcripts encode $VEGF_{121}$, which has a 44 amino acid deletion between positions 116 and 159 of $VEGF_{165}$, $VEGF_{189}$, which has 24 amino acids inserted at position 116, and $VEGF_{206}$, which has 41 amino acids inserted at position 116 (Tischer *et al.*, 1991).

Two tyrosine kinases, fms-like tyrosine kinase (*flt-1*) and the kinase insert domain-containing receptor (KDR) have been identified as the high affinity receptors for VEGF (de Vries *et al.*, 1992; Terman *et al.*, 1992). The murine homologue of KDR is *flk-1*, whose sequence is 85% identical with that of KDR. The *flt-1* and KDR genes encode tyrosine kinase receptors consisting of an extracellular domain containing seven immunoglobulin domains, a transmembrane domain and a split tyrosine kinase intracellular domain (Shibuya *et al.*, 1990).

The longer forms of VEGF bind heparin through a site that appears to be distinct from the receptor-binding domain (Vaisman *et al.*, 1990). The heparin binding site is located in the basic C-terminal region of the longer forms of VEGF since $VEGF_{165}$ can be cleaved by plasmin to yield $VEGF_{110}$, which lacks residues 111–165 and has no affinity for heparin (Park *et al.*, 1993). Since the sequence of residues 1–110 displays limited but significant homology (19%) to that of PDGF, this suggests that the first 110 residues of VEGF fold independently to form a PDGF-like domain that binds to the VEGFR while the 55 C-terminal residues form the heparin-binding domain. $VEGF_{121}$ lacks this basic region and does not bind heparin but can trigger angiogenesis and vascular permeability (Houck *et al.*, 1992; Kondo *et al.*, 1995).

The carboxy-terminal peptide (residues 111–165) produced by plasmin cleavage of $VEGF_{165}$ has no affinity for soluble KDR or *flt-1* receptors (Keyt *et al.*, 1996a). $VEGF_{110}$ binds to soluble KDR with similar affinity to $VEGF_{165}$ and $VEGF_{121}$ in the absence of heparin (Keyt *et al.*, 1996a). By contrast, $VEGF_{121}$ and $VEGF_{110}$ bind to *flt-1* with 10–20-fold decreased affinity compared with $VEGF_{165}$ (Keyt *et al.*, 1996a). A $VEGF_{165}/VEGF_{110}$ heterodimer has an affinity for *flt-1* intermediate between $VEGF_{110}$ and $VEGF_{165}$ homodimers (Keyt *et al.*, 1996a). These results show that the C-terminal domain of VEGF contains determinants for binding to *flt-1* even though the 55 amino acid peptide by itself has no detectable affinity for *flt-1*.

In addition to VEGF, placenta growth factor (PIGF) has been shown to bind to *flt-1* with high affinity, but not to KDR (Kendall *et al.*, 1994). PIGF induces procoagulant tissue factor

production by monocytes and endothelial cells and is a very weak stimulator of endothelial cell chemotaxis and proliferation (Clauss *et al.*, 1996). The sequence of PlGF is 47% identical with that of VEGF. Alternate splicing of mRNA for PlGF generates two variants containing 132 and 153 amino acids (Maglione *et al.*, 1993), known as PlGF-1 and PlGF-2, respectively. The insertion of a 21 amino acid basic region near the C-terminus of the longer form confers heparin-binding ability on it (Hauser and Weich, 1993).

The active forms of VEGF and PlGF are dimeric; in addition to VEGF and PlGF homodimers, a heterodimer of VEGF and PlGF has been purified and characterized (DiSalvo *et al.*, 1995). Heterodimers composed of combinations of $VEGF_{121}$, $VEGF_{165}$, PlGF-1 and PlGF-2 have been synthesized *in vitro* from monomers and shown to have mitogenic activity (Birkenhager *et al.*, 1996). That the various heterodimers are biologically active suggests that the determinants of dimerization are located in the first ~110 residues of VEGF and PlGF. Homodimeric PlGF has very weak mitogenic activity compared with homodimeric VEGF and the VEGF/PlGF heterodimer (DiSalvo *et al.*, 1995); this is possibly because the KDR/*flk-1* receptor can transduce a mitogenic signal while activation of the *flt-1* receptor does not seem to produce a similar response (de Vries *et al.*, 1992; Millauer *et al.*, 1994).

The VEGF and PlGF genes display a limited sequence similarity to that of platelet-derived growth factor (PDGF), a member of the cystine knot growth factor family that also includes transforming growth factor β (TGFβ), nerve growth factor (NGF) and chorionic gonadotropin (CG) (McDonald and Hendrickson, 1993). The characteristic fold of this family is a pair of twisted antiparallel β sheets linked by a cystine knot formed by three disulphide bonds (Murray-Rust *et al.*, 1993). One of the disulphide bonds penetrates a ring formed by the other two bonds and the backbone atoms linking them. The sequence similarity in the family is low but the residues involved in the cystine knot are conserved. The structures are most similar about the knot and diverge rapidly from each other as the distance from the knot increases. The β strands have similar hydrogen-bonding patterns in each structure. The cystine knot growth factors are dimeric *in vivo* but the mode of dimerization is different in each case. The mechanism of action is thought to involve ligand-induced dimerization of the tyrosine kinase receptors.

The cysteines involved in forming the cystine knot are conserved in the sequences of VEGF and PlGF. Two other cysteines that are essential for dimerization of PDGF are also conserved in VEGF and PlGF. These cysteines have been shown to be essential for the dimerization and biological activity of VEGF (Potgens *et al.*, 1994).

Because of the low sequence similarity among the cystine knot growth factors, a comparison of the sequences of VEGF and PlGF with those of PDGF-A and PDGF-B gives little insight into the receptor-binding determinants. Alanine-scanning mutagenesis has been used to identify charged residues involved in VEGF binding to *flt-1* and KDR (Keyt *et al.*, 1996b). VEGF binding to KDR/*flk-1* is mediated by a positively charged surface while binding to *flt-1* is due to negatively charged residues. A model of VEGF based on the structure of PDGF shows that these residues are clustered in loops at opposite ends of the VEGF dimer (Keyt *et al.*, 1996b). This model was constructed by aligning the sequence of VEGF with that of PDGF and substituting the side chains of the charged residues involved in receptor binding for the corresponding residues in PDGF.

In the present work, models of the PDGF-like domains of VEGF and PlGF have been built by homology modelling using the crystallographic structure of PDGF-BB as a template. Deletions in the loop regions were modelled using database searching and a systematic classification of β hairpin structures (Sibanda *et al.*, 1989). The models were refined using energy minimization and molecular dynamics. The correctness of the models was assessed by evaluating the compatibility of the sequences with the cystine knot fold. This was done by comparing the models with their sequences using a 3D profile computed from the atomic coordinates of the models and calculating the compatibility of each residue in the sequence with the environment defined by its position in the profile. The sum of the compatibility scores over all residues in the sequence gives the self-compatibility score; it has been shown that the 3D profiles of correct protein structures match their sequences with high self-compatibility scores (Luthy *et al.*, 1992).

Given the receptor-binding affinity of $VEGF_{110}$, this model should contain all the determinants of KDR binding and the most important determinants of *flt-1* binding. The model of VEGF is consistent with the available data on the residues that mediate receptor binding. No corresponding data for PlGF are available at the time of writing. It is hoped that the models will stimulate and guide further work to identify the residues that determine receptor binding in VEGF and PlGF. The models suggest an explanation for the difference in receptor-binding specificity of VEGF and PlGF.

Materials and methods

The X-ray structure of PDGF-BB at 3.0 Å resolution was used as the basis of the models (Oefner *et al.*, 1992). Monomer A of the PDGF structure was used as the template since this contains the more complete set of coordinates. Sequences were aligned using Clustal (Higgins and Sharp, 1988) and manually adjusted to preserve the β sheet structure (Figure 13). Molecular graphics and model building were done using the InsightII software package (Biosym Technologies, 1994) running on a Silicon Graphics Indy workstation. Attempts to predict the secondary structure of VEGF and PlGF using the PredictProtein (Rost, 1996) and SOPM algorithms (Geourjon and Deleage, 1995) did not produce useful information.

The PDGF(A) structure corresponds to residues 19–109 of VEGF/PlGF. There are no coordinates for the residues in PDGF(A) corresponding to residues 38–44 of VEGF/PlGF. This is due to proteolytic cleavage in this region of PDGF, which makes it impossible to resolve the structure of loop I. The Homology module of the InsightII package was used to build coordinates for residues 17–37, 45–83 and 89–109, using PDGF(A) as the basis. Loop II (residues 62–64) is the same length in PDGF and VEGF/PlGF, so this loop was built using the loop from PDGF. Loops I and III were built by database searching using the Homology module. Loop III (residues 84–88) is a β hairpin in the growth factors and was modelled using the published systematic classification of β hairpins (Sibanda *et al.*, 1989) as a guide. Each loop was chosen to have a minimum root mean square (r.m.s.) distance between the tails of the loop and the sheets and to have the maximum sequence similarity with VEGF/PlGF. In addition, the compatibility of residues in the loop with the environments provided by the fragments was assessed using the Profiles program. The

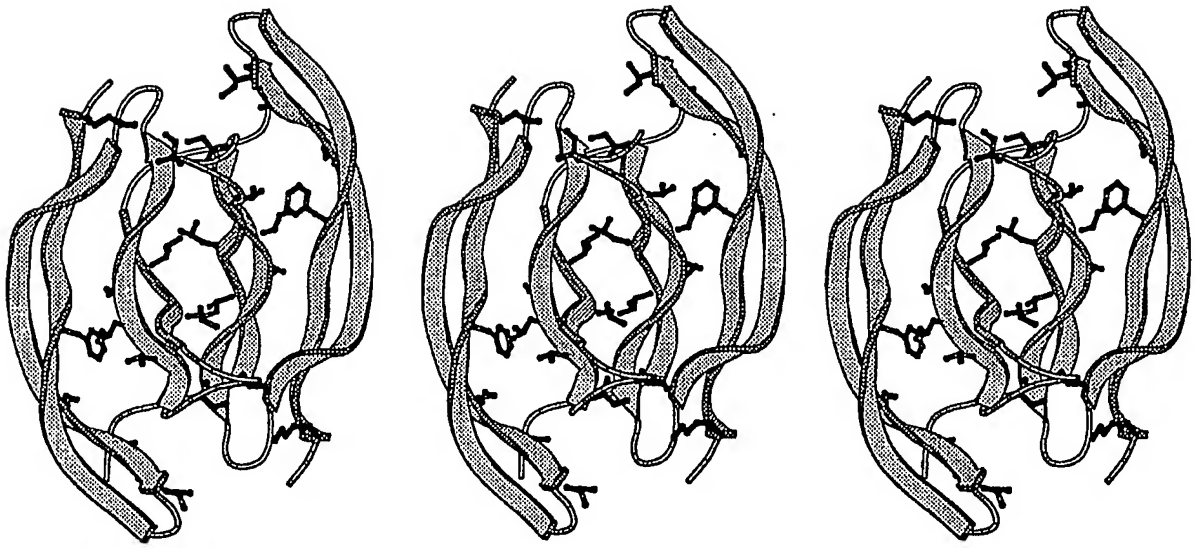

Fig. 1. MOLSCRIPT (Kraulis, 1991) stereo drawing of the VEGF dimer. Hydrophobic residues in the dimer interface are drawn in ball-and-stick representation.

models were not refined before being tested by Profiles since experience has shown that refinement does not substantially improve the profile of a loop that is misfolded in the unrefined model.

The disulphide bonds in the cystine knot were formed between Cys26–Cys68, Cys57–Cys102 and Cys60–Cys104. A dimeric model was constructed in the same orientation as the PDGF dimer and intersubunit disulphide bonds formed between Cys51 and Cys60. This seemed the most likely orientation because the Cys residues involved in the intersubunit disulphide bond are conserved in VEGF and PIGF and it has been shown by site-directed mutagenesis of these Cys residues that a similar pair of disulphide bonds is necessary for the dimerization and biological activity of VEGF (Potgens *et al.*, 1994).

The bond lengths and angles at the splice points where loops were added were refined using the Splice Repair facility of the Homology module. All residues except the two next to the splice points were fixed, a torsion force was placed on the ω angles of the peptide bonds at the splice point and 100 steps of steepest descent minimization were performed. The conformations of mutated side chains were then adjusted using an automated procedure that minimizes the energy of side chain conformations by a systematic search of rotamer conformations.

A Profiles (Luthy *et al.*, 1992) analysis of the unrefined VEGF model showed that residues 17 and 18 were in very incompatible environments. These hydrophobic residues may interact with the heparin-binding domain. These hydrophobic residues lie on the opposite face of the dimer to the receptor-binding loops and they may interact with the heparin-binding domain. Residues 17 and 18 were cut from the model and the dimer was re-refined.

The dimeric model was solvated with a 9 Å shell of TIP3P water (Jorgensen *et al.*, 1983). Molecular mechanics and dynamics were performed using CHARMM with a united atom forcefield (Brooks *et al.*, 1983). The solvated model was energy minimized using the Adopted Basis Newton–Raphson algorithm with the CHARMM forcefield (Brooks *et al.*, 1983). Initially only hydrogens were minimized, then water molecules, followed by side chains and then the entire model. The model was then subjected to molecular dynamics. A 1 fs time step was used throughout the molecular dynamics simulation. The non-bonded cut-off distance was 8 Å and the dielectric was distance dependent. The solvated model was heated from 0 to 300 K over 1 ps and then equilibrated for 10 ps. This was followed by free dynamics at 300 K for 25 ps. Bonds involving hydrogen atoms were constrained. The model was then quenched from 300 to 0 K over 1 ps and reminimized without constraints.

Stereochemical analysis of the models was performed using PROCHECK (Laskowski *et al.*, 1993). The quality of the models was assessed using Profiles (Luthy *et al.*, 1992). Electrostatic potential grids were created using DelPhi (Sharp and Honig, 1990). All protein charges were taken from the AMBER charge templates provided with the DelPhi program (Sharp and Honig, 1990).

Results and discussion

MOLSCRIPT diagrams of VEGF and PIGF are shown in Figures 1 and 2. The dimer structure is similar to that in PDGF but is more curved along the long axis (Figures 3 and 4). The r.m.s differences were calculated between the starting and refined structures (Table 1). These indicate that the refined structures have changed somewhat from the initial structure. The side chain r.m.s. differences are large since the sequence identity between PDGF and VEGF/PIGF is low and the dimer lacks a hydrophobic core in which the conformational flexibility of the side chains would be restricted. A comparison of the structures of PDGF, TGFβ2 and NGF shows that their backbones diverge rapidly from each other away from the cystine knot. It seems reasonable, therefore, that the backbones of the refined VEGF/PIGF models diverge from that of the PDGF template. Ramachandran plots of the backbone angles (Figures 5 and 6) in the models show that they fall into commonly

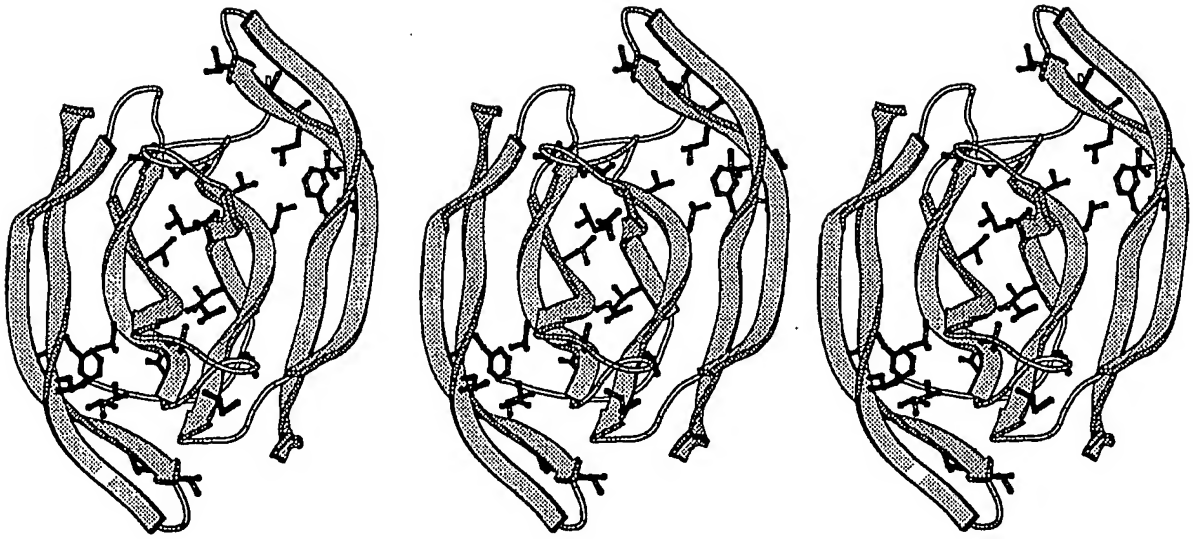

Fig. 2. MOLSCRIPT stereo drawing of the PIGF dimer. Hydrophobic residues in the dimer interface are drawn in ball-and-stick representation.

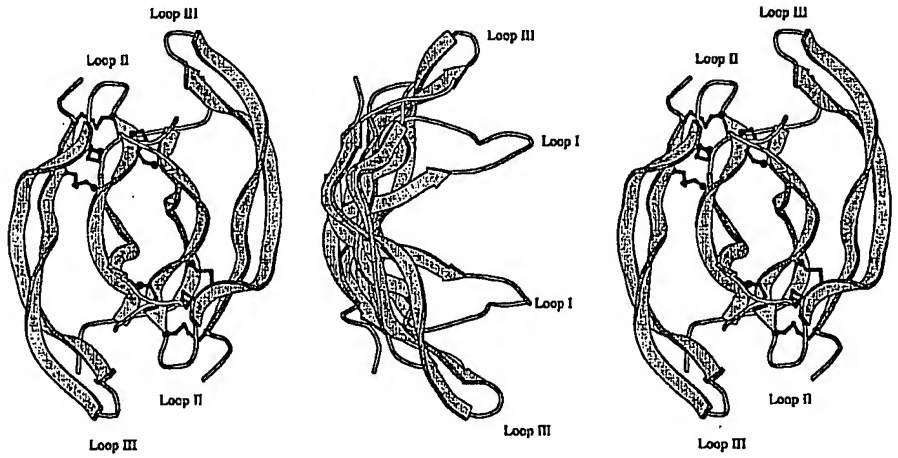

Fig. 3. Ribbon diagrams of the VEGF dimer related by a 90° rotation, drawn using MOLSCRIPT. The cysteine residues that form the cystine knot and the intersubunit disulphide bonds are drawn as balls and sticks.

observed regions of ϕ-ψ space. The conserved glycine in the cystine knot has a positive ϕ conformation as is observed in PDGF and TGFβ2. The disulphide bonds in the cysteine knot have similar conformations to those in PDGF. The β bulge preceding Cys97 in PDGF is also present before Cys102 in VEGF and PIGF. The dimer has the shape of a shallow trough with loop I projecting from the concave surface. The structure of loop I was built based on the structure of residues A39–A48 of PDB entry 3rp2. The systematic classification of β hairpins (Sibanda *et al.*, 1989) predicts that the deletion of three residues in loop II will change the class 2:2I' hairpin in loop II of PDGF to a class 3:5 hairpin. Loop II was built using a class 3:5 hairpin from 1sgt (Figure 7). The hydrogen bonding pattern in the β sheets is similar to that in PDGF. There are two hydrogen bonds between Lys32 and Met65 (Ser30 and Leu63 in PIGF), causing a bulge in the β strand following loop I. Mutation of Met65 (Leu63 in PIGF) to a non-hydrophobic residue may change the positions of loops I and II relative to each other since this residue is buried along the interface between the loops. The twofold symmetry of the dimer causes the clustering of the loops at the ends of the dimer. In the other cystine knot growth factors the residues involved in receptor binding are located in the loops. If this is the case in PIGF and VEGF, then the loops will form two identical binding regions at opposite ends of the dimer that could bind two receptor molecules and induce receptor dimerization and activation. Mutations in loop I of PDGF do not disrupt the structure of the rest of the protein and this may also be the case in VEGF/PIGF, since this loop points into the solvent and does not interact with the body of the protein.

It has been shown that VEGF is only active in the dimeric form and that dimerization is dependent on the formation of an intersubunit disulphide bond between Cys51 of one subunit and Cys60 of the other (Potgens *et al.*, 1994). Mutants lacking

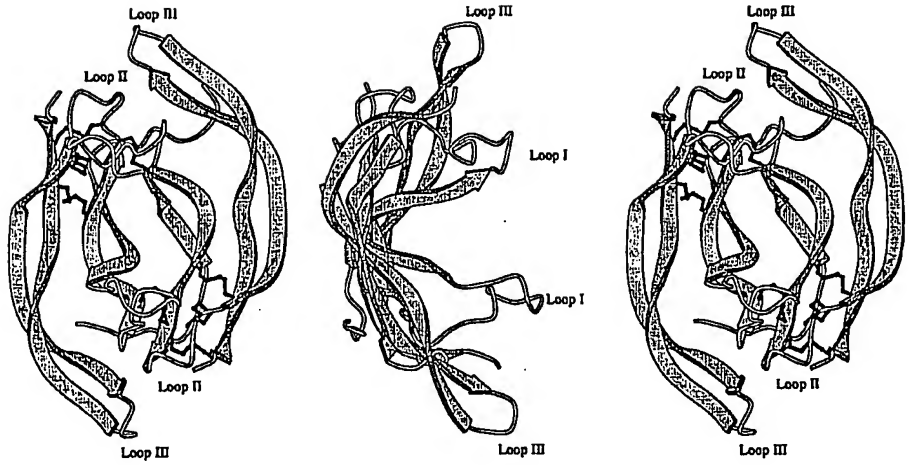

Fig. 4. Ribbon diagrams of the PIGF dimer related by a 90° rotation, drawn using MOLSCRIPT. The cysteine residues that form the cystine knot and the intersubunit disulphide bonds are drawn as balls and sticks.

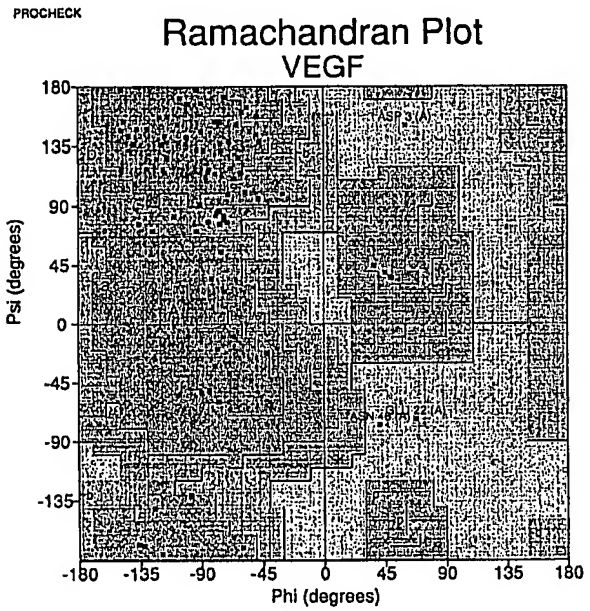

Fig. 5. Ramachandran plot for VEGF, prepared using PROCHECK.

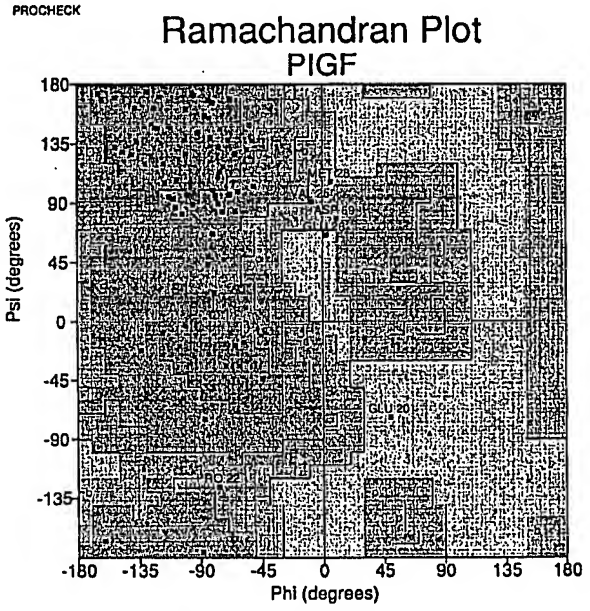

Fig. 6. Ramachandran plot for PIGF, prepared using PROCHECK.

either of these Cys are unable to form dimers. The coexpression of Cys51→Ser51 mutants with Cys60→Ser60 mutants leads to formation of heterodimers that are fully active despite having only one intersubunit disulphide bond.

The cysteine knot is formed by the disulphide bonds Cys26–Cys68, Cys57–Cys102 and Cys61–Cys104. These disulphide bonds have similar conformations to those in PDGF. The mutation of any one of Cys26, Cys57, Cys61 or Cys68 to a Ser residue results in impaired dimerization (Potgens *et al.*, 1994; Claffey *et al.*, 1995). This cannot be due to disruption of an intersubunit disulphide bond involving these Cys residues since they are not in a position to form disulphide bonds with any of the Cys residues in the symmetry-related subunit. These mutations disrupt the structure of the cystine knot, causing a change in the position of Cys60, which is located within the backbone ring of the knot. Cys26 forms one half of the disulphide bond that penetrates the ring of the cystine knot; mutation of Cys26 may disrupt the tight packing in the knot. One study (Potgens *et al.*, 1994) found that the mutant Cys57→Ser57 can still form dimers at the level of 50% of the wild type and that these dimers are biologically active but another (Claffey *et al.*, 1995) found that, like the other mutants, this mutant is unable even to dimerize. Cys57 is at the end of β strand 2 next to loop II and may be less crucial to the integrity of the fold; mutants at this site might still be correctly folded and able to form noncovalent dimers. It is interesting that Claffey *et al.* (1995) found that the mutation Cys102→Ser prevents the synthesis and/or secretion of this isoform. In addition, this isoform is a dominant-negative mutant that limits the synthesis and/or secretion of wild-type VEGF. This suggests

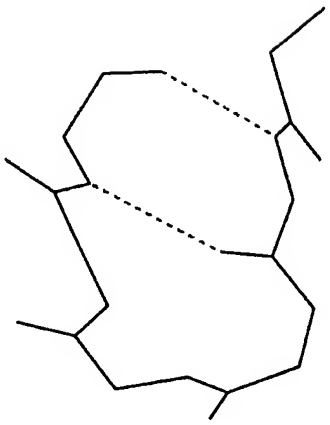

Fig. 7. Backbone structure of the loop from PDB entry 1sgt that was used to model loop III. Dotted lines indicate hydrogen bonds.

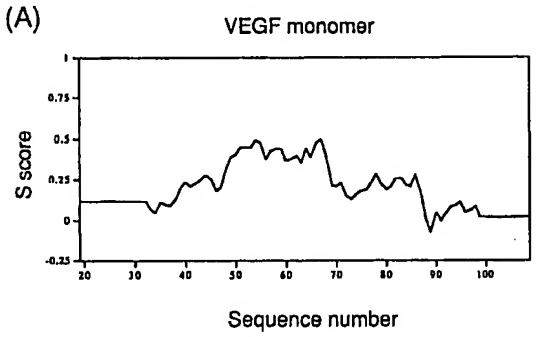

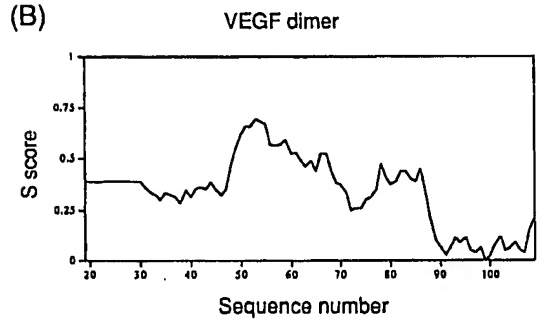

Fig. 8. Profile plots for the monomeric (A) and dimeric (B) forms of VEGF. A self-compatibility score (S) is determined for each residue in the sequence. The compatibility of the sequence with the structure can be assessed by plotting the S score against residue number in a window. Negative S scores indicate putatively misfolded regions. A smoothing window size of 21 residues is used and scores for the first ten and last ten residues have no significance.

that the Cys102→Ser mutant can form a heterodimer with normal VEGF that is subsequently degraded intracellularly.

The stability of the dimer may also be affected by inter-

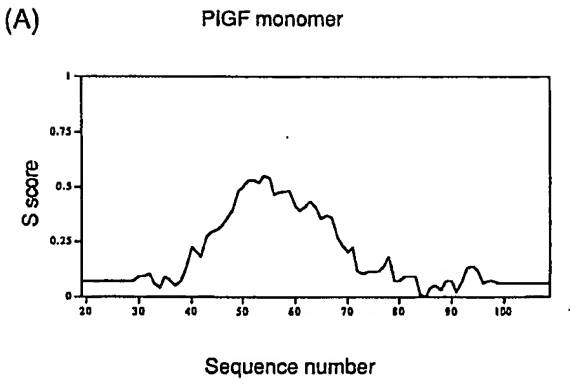

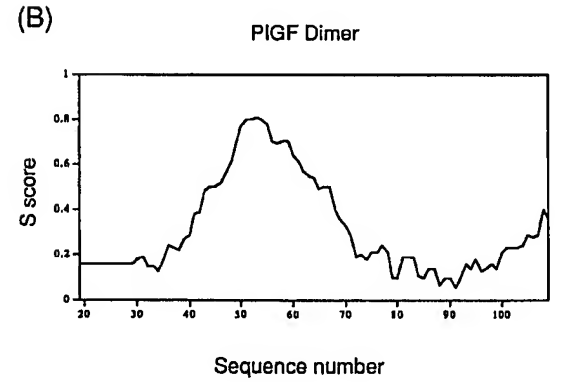

Fig. 9. Profile plots for the monomeric (A) and dimeric (B) forms of PIGF. See the legend to Figure 8 for an explanation of the plot.

subunit hydrogen bonding. There are several charge pairs buried along the dimer interface: in VEGF Lys48 forms charge pairs with Asp63 of the other monomer while Arg82 forms a charge pair with Glu64. In PIGF there are charge pairs formed by Lys82 with Glu64 and Glu30 with Arg27. A striking feature of the models is that almost none of the hydrophobic residues have more than 90% of their accessible surface area buried in the interior of the protein. The only exception is Val52, which is completely buried (0% of surface area accessible to solvent) in both VEGF and PIGF. This is adjacent to Cys51 and the burial of this residue may play a part in determining the conformation of the cystine knot. However, dimer formation does bury some hydrophobic surface area, as can be seen from a comparison of the profiles of the monomeric and dimeric forms of VEGF and PIGF (Figures 8 and 9). Hydrophobic residues involved in the dimer interface are listed in Table II. The residues at positions 20, 29, 43, 46, 52, 78, 81, 83 and 96 are involved in the dimer interface in both proteins. A model of the VEGF/PIGF heterodimer might provide further insights into the requirements for dimerization. The models show that the PDGF-like domains of VEGF and PIGF are essentially two-dimensional structures that lack a hydrophobic core.

The Profiles suite of programs (Luthy *et al.*, 1992) was used to assess the quality of the models. Profiles measures the compatibility of each residue in a model with its environment and calculates a Z score that is a measure of the compatibility

Fig. 10. Solvent-accessible surfaces of the VEGF (A) and PIGF (B) monomers coloured according to the electrostatic energy at each point on the surface. The energies were taken from an electrostatic grid calculated using the DelPhi module in InsightII. The units of the spectrum are *kT*.

of the entire sequence with the fold of the model. Correctly folded proteins have a *Z* score at least 45% of the maximum theoretically possible score (the *S* score). The dimeric VEGF model has a *Z* score that is 57% of the *S* score. The residue by residue profile (Figures 8 and 9) does not indicate any misfolded regions although the scores for loops I and III are low. The dimeric PIGF model has a *Z* score that is 70% of the *S* score. While it is possible that the N-terminal region of the domain that could not be modelled interacts with the part modelled here, the *Z* scores and the profiles indicate that the fold is basically correct. The areas of greatest error are likely to be the loops, especially the large loop I. A comparison of the profiles of the dimeric and monomeric models (Figures 8 and 9) shows that dimer formation improves the scores along the dimeric interface by burying hydrophobic residues. Dimerization buries about 900 Å^2 of surface area per monomer. Of this, about 380 Å^2 is buried along the dimer interface; this is less than in PDGF. Unlike PDGF, VEGF is unable to form stable, biologically active noncovalent dimers. This may be because the smaller surface area buried in VEGF is insufficient to stabilize the dimer in the absence of intersubunit disulphide bonds. By contrast, the NGF dimer, which is non-covalent, buries 1166 Å^2 of surface area per monomer.

The receptor-binding domains of $VEGF_{206}$ have been studied using monoclonal antibodies raised against peptides from the sequence of $VEGF_{206}$ (Sioussat *et al.*, 1993). Using the Chou and Fasman (1978) algorithm, peptides were predicted to contain elements of regular secondary structure. The study identified the N- and C-termini of $VEGF_{206}$ as being important in receptor binding. If the models presented are correct then none of the peptides used would include complete loops and the β strands joined by the loops. Since antibodies to proteins are generally formed against three-dimensional structure rather than sequence, antibodies raised against the peptides used in this study would not recognize the loop regions. None of the available secondary structure predictors is able to predict accurately the secondary structure of the cystine knot growth factors and are therefore not useful guides to designing peptides for a study of this kind.

DelPhi calculations of the electrostatic potential over the surface of the dimers reveal a number of differences in the distribution of positive and negative charges (Figure 10). Loop

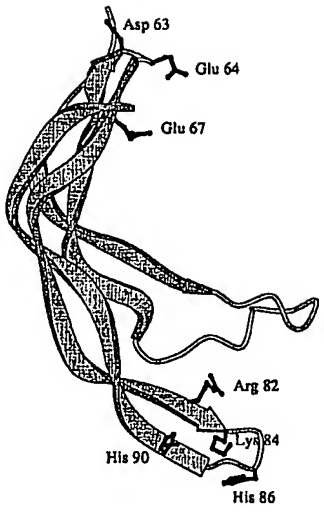

Fig. 11. MOLSCRIPT ribbon diagram of the VEGF monomer. Residues in the loops that are postulated to be involved in receptor binding are drawn in ball-and-stick representation.

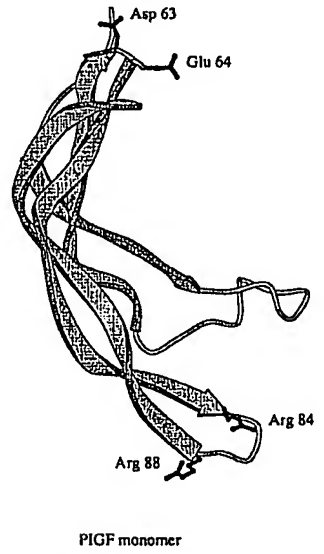

Fig. 12. MOLSCRIPT ribbon drawing of the PIGF monomer with residues postuluted to be involved in receptor binding drawn in ball-and-stick representation.

I in VEGF contains a large, elongated negatively charged region formed by Asp34, Gln37, Glu38, Pro40, Asp41, Glu42 and Glu44, whereas this loop in PIGF is almost uncharged. The body of the PIGF dimer contains a large area of positive charge consisting of Arg55, His99, Arg31, His67, Pro70 and Ser97, which is absent in VEGF. The residues Lys84, His86 and His90 in VEGF form an elongated positively charged patch at the tip of loop III. The corresponding hairpin in PIGF has a positively charged surface formed by the side chains of Arg84 and Arg88 (Figures 10 and 12); this surface is smaller than that in VEGF. This loop also includes a negatively charged side chain, Asp87; the corresponding residue in VEGF is Gln. In both VEGF and PIGF, loop II has a negatively charged patch formed by Asp63, Glu64 and Glu67 in VEGF and by Asp63 and Glu64 in PIGF.

There are several patches of exposed hydrophobic residues on the surfaces of VEGF and PIGF. The residues Met81, Ile83 and Ile91 form a hydrophobic patch on the surface of loop III in VEGF. In PIGF the residue corresponding to Met81 (Leu81) is buried and Ile91 is replaced by a Tyr residue, resulting in a much smaller hydrophobic patch formed by Ile83. The conserved Leu66 is exposed in both VEGF and PIGF. There is a large area of hydrophobic surface formed at the interface of loops I and II by Val33, Val35, Phe37, Leu80 and Val92 in PIGF and by Val33, Ile35, Phe37 and Ile80 in VEGF.

The charged residues in VEGF that are involved in receptor binding have been identified by alanine-scanning mutagenesis. Arg82, Lys84 and His86 in VEGF are critical for binding to KDR/*flk-1* while Asp63, Glu64 and Glu67 were implicated in binding to *flt-1* and to a lesser extent, KDR (Keyt *et al.*, 1996). A model of VEGF was constructed by aligning the sequences of VEGF and PDGF and substituting the side chains of these charged residues for the corresponding residues in PDGF. This model does not contain coordinates for loop 1 and was not subjected to refinement by energy minimization or molecular dynamics. The backbone structure of this model is identical with that of PDGF. The model of VEGF presented here shows that the backbones of VEGF and PDGF diverge significantly from each other outside the region of the cystine knot.

This model locates the positively charged residues Arg82, Lys84 and His86 in a cluster on the edge of the loop III β hairpin. The model presented here shows that the side chains of Arg82, Lys84, His86 and His90 form a positively charged surface on the plane of the β hairpin, with His86 forming part of the β hairpin (Figures 10 and 11). Although His90 forms part of this positively charged surface mutation of this residue to Ala has little effect on binding. The position of the negatively charged residues Asp63, Glu64 and Glu67 is similar in both models. The potential extra glycosylation site introduced by mutation of Glu64 is located at the tip of loop II, which mediates binding to *flt-1*. Glu64 is one of the residues implicated in binding to *flt-1*; it is therefore not surprising that mutation of this residue to Asn reduces binding to *flt-1* ~40-fold. No effect on binding to either *flt-1* or KDR was detected by mutagenesis of charged residues in loop I. The comparison of the models of VEGF and PIGF suggests that the inability of PIGF to bind KDR may be due to differences in the positively charged surface in loop III of PIGF as compared with VEGF and the absence of exposed hydrophobic residues in loops I and II. The ability of PIGF to bind *flt-1* is consistent with the presence of a negatively charged surface in loop II similar to the one that mediates VEGF binding to *flt-1*.

VEGF has a putative N-linked glycosylation site with the consensus sequence Asn–Thr–Leu, at residues 75–77. Mutation of Asn75 to Tyr alters the electrophoretic mobility of the VEGF dimer, consistent with a lack of glycosylation (Claffey *et al.*, 1995). The VEGF model shows that the side chain of Asn75 is exposed to solvent and is located near the middle of the fourth β strand (Figure 11). Mutation of this site has no effect on receptor-binding activity (Claffey *et al.*, 1995), which is not surprising given that it is not located near the receptor-binding loops. The site is conserved in PIGF.

It is hoped that the models presented here will be useful

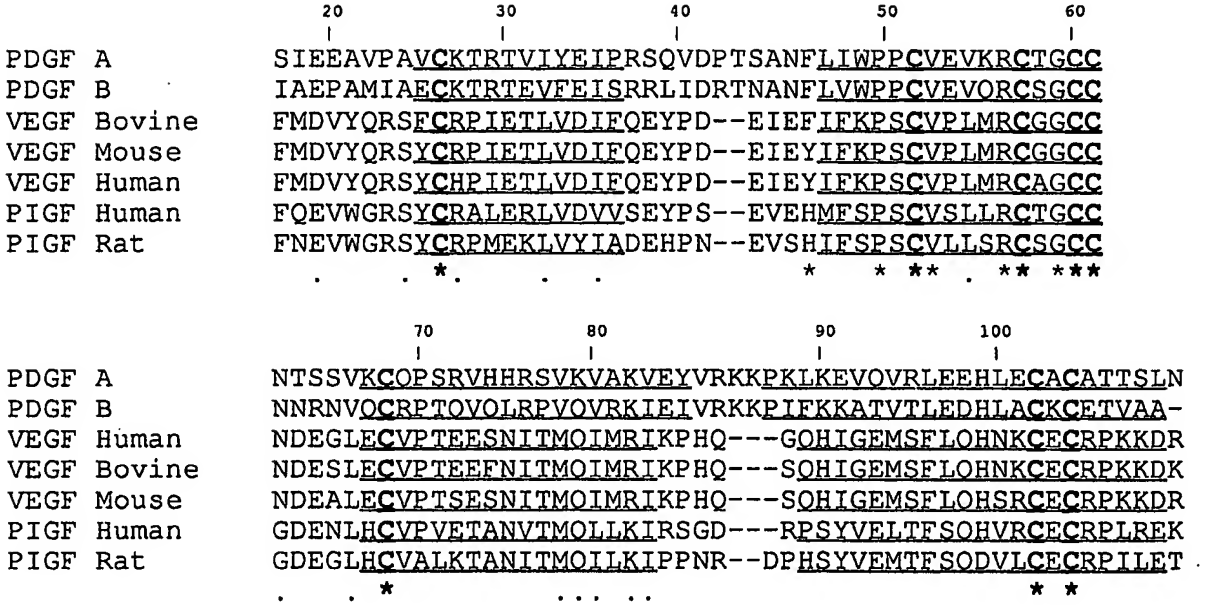

Fig. 13. Clustal sequence alignment of the sequences of human PDGF-A and PDGF-B, human, bovine and mouse VEGF and human and rat forms of PIGF. The alignment begins at residue 19 of the mature VEGF sequence and ends at residue 109 of that sequence. This is the region of VEGF corresponding to the model. Cysteine residues involved in the cystine knot are in bold type. Conserved residues are marked by an asterisk and conservative substitutions by a period (.). Residues underlined are in the β sheets.

Table I. Root mean square differences between starting and refined structures of PIGF and VEGF

	Atom selection	R.m.s.d. (Å)
PIGF	All non-hydrogen atoms	3.53
	Backbone atoms	1.64
	α-Carbon atoms	1.60
VEGF	All non-hydrogen atoms	2.13
	Backbone atoms	1.90
	α-Carbon atoms	1.82

Table II. Hydrophobic residues with surface area buried in the dimer interfaces of VEGF and PIGF

VEGF	PIGF
Val20	Val20
Ile29	Leu29
Leu32	Leu32
Phe36	
Ile43	Val43
Val52	Val52
Leu54	Leu54
	Leu55
Met78	Met78
Ile80	
Met81	Leu81
Ile83	Ile83
Ile91	
Met94	
Phe96	Phe96

as guides to the design of future mutagenesis experiments. Modelling of the receptors is in progress. In combination with models of the receptors, the models of VEGF and PIGF will be used to investigate the determinants of receptor binding. An understanding of these would be a first step towards the rational design of VEGF inhibitors which might prove useful as inhibitors of angiogenesis and tumour growth

Acknowledgements

Financial support for this work was provided by the Association for International Cancer Research and the Irish Cancer Society. T.P.W. is grateful to the Irish Cancer Society for a studentship.

References

Biosym Technologies (1994) *InsightII User Guide, Version 2.3.5.* Biosym Technologies, San Diego, CA.
Birkenhager,R., Schneppe,B., Rockl,W., Wilting,J., Weich,H.A. and McCarthy,J.E.G. (1996) *Biochem. J.*, 316, 703–707.
Brooks,B.R., Bruccoleri,R., Olafson,B.D., States,D.J., Swaminathan,S. and Karplus,M. (1983) *J. Comput. Chem.*, 4, 187–217.
Chou,P.Y. and Fasman,G. (1978) *Adv. Enzymol.*, 47, 45–148.
Claffey,K.P., Senger,D.R. and Spiegelman,B.M. (1995) *Biochim. Biophys. Acta*, 1246, 1–9.
Clauss,M., Weich,H., Breier,G., Knies,U., Rockl,W., Waltenberger,J. and Risau,W. (1996) *J. Biol. Chem.*, 271, 17629–17634.
de Vries,C., Escobedo,J.A., Ueno,H., Houck,K., Ferrara,N. and Williams,L.T. (1992) *Science*, 255, 989–991.
DiSalvo,J., Bayne,M.L., Conn,G., Kwok,P., Trivedi,P.G., Soderman,D.D., Palisi,T.M., Sullivan,K.A. and Thomas,K.A. (1995) *J. Biol. Chem.*, 270, 7717–7723.
Ferrara,N. and Henzel,W.J. (1989) *Biochem. Biophys. Res. Commun.*, 161, 851–858.
Ferrara,N., Winer,J., Burton,T., Rowland,A., Siegel,M., Phillips,H.S., Terrell,T., Keller,G.A. and Levinson,A.D. (1993) *J. Clin. Invest.*, 91, 160–170.
Folkman,J. (1971) *N. Engl. J. Med.*, 285, 1182–1186.
Geourjon,C. and Deleage,G. (1995) *Protein Engng*, 7, 157–164
Hauser,S. and Weich,H.A. (1993) *Growth Factors*, 9, 259–268.
Higgins,D.G. and Sharp,P.M. (1988) *Gene*, 73, 237–244.
Houck,K.A., Ferrara,N., Winer,J., Cachianes,G., Li,B. and Leung,D.W. (1991) *Mol. Endocrinol.*, 5, 1806–1814.

Houck,K.A., Leung,D.W., Rowland,A.M., Winer,J. and Ferrara,N. (1992) *J. Biol. Chem.*, **267**, 26031–26037.
Jorgensen,W.L., Chandrasekhar,J., Madura,J.D., Impey,R.W. and Klein,M.L. (1983) *J. Chem. Phys.*, **79**, 926–935.
Kendall,R.L., Wang,G., DiSalvo,J. and Thomas,K.A. (1994) *Biochem. Biophys. Res. Commun.*, **201**, 326–330.
Keyt,B.A., Berleau,L.T., Nguyen,H.V., Chen,H., Heinsohn,H., Vandlen,R. and Ferrara,N. (1996a) *J. Biol. Chem.*, **271**, 7788–7795.
Keyt,B.A., Nguyen,H.V., Berleau,L.T., Duarte,C.M., Park,J., Chen,H. and Ferrara,N. (1996b) *J. Biol. Chem.*, **271**, 5638–5646.
Kim,K.J., Li,B., Winer,J., Armanini,M., Gillett,N., Phillips,H.S. and Ferrara,N. (1993) *Nature*, **362**, 841–844.
Kondo,S., Matsumato,T., Yokoyama,Y., Ohmori,I. and Suzuki,H. (1995) *Biochim. Biophys. Acta*, **1243**, 195–202.
Kraulis,P. (1991) *J. Appl. Crystallogr.*, **24**, 946–950.
Laskowski,R.A., MacArthur,M.W., Moss,D.S. and Thornton,J.M. (1993) *J. Appl. Crystallogr.*, **26**, 283–291.
Luthy,R., Bowie,J.U. and Eisenberg,D. (1992) *Nature*, **356**, 83–85.
Maglione,D. *et al.* (1993) *Oncogene*, **8**, 925–931.
McDonald,N.Q. and Hendrickson,W.A. (1993) *Cell*, **73**, 421–424.
Millauer,B., Shawver,L.K., Plate,K.H., Risau,W. and Ullrich,A. (1994) *Nature*, **367**, 576–579.
Murray-Rust,J., McDonald,N.Q., Blundell,T.L., Hosang,M., Oefner,C., Winkler,F. and Bradshaw,R.A. (1993) *Structure*, **1**, 153–159.
Oefner,C., D'Arcy,A., Winkler,F.K., Eggiman,B. and Hosang,M. (1992) *EMBO J.*, **11**, 3921–3926.
Park,J.E., Keller,G.A. and Ferrara,N. (1993) *Mol. Cell. Biol.*, **4**, 1317–1326.
Plate,K.H., Breier,G., Weich,H.A. and Risau,W. (1992) *Nature*, **359**, 845–848.
Potgens,A.J.G., Lubsen,N., van Altena,M.C., Vermeulen,R., Bakker,A., Schoenmakers,J.G.G., Ruiter,D.J. and de Waal,R.M.W. (1994) *J. Biol. Chem.*, **269**, 32879–32885.
Rost,B. (1996) *Methods Enzymol.*, **266**, 525–539.
Sharp,K.A. and Honig,B. (1990) *Annu. Rev. Biophys. Biophys. Chem.*, **19**, 301–332.
Shibuya,M., Yamane,A., Ikeda,T., Tojo,A., Matsushime,H. and Sato,M. (1990) *Oncogene*, **5**, 519–524.
Shweiki,D., Itin,A., Soffer,D. and Keshet,E. (1992). *Nature*, **359**, 843–845.
Sibanda,B.L., Blundell,T.L. and Thornton,J.M. (1989) *J. Mol. Biol.*, **206**, 759–777.
Sioussat,T.M., Dvoruk,H.F., Brock,T.A. and Senger,D.R. (1993) *Arch. Biochem. Biophys.*, **301**, 15–20.
Terman,B.I., Dougher-Vermuzen,M., Carrion,M.E., Dimitrov,D., Armellino,D.C., Gospodarowicz,D. and Bohlen,P. (1992) *Biochem. Biophys. Res. Commun.*, **187**, 1579–1586.
Tischer,E., Mitchell,R., Hartman,T., Silva,M., Gospodarowicz,D., Fiddes,J.C. and Abraham,J.A. (1991) *J. Biol. Chem.*, **266**, 11947–11954.
Vaisman,N., Gospodarowicz,D. and Neufeld,G. (1990) *J. Biol. Chem.*, **265**, 19461–19466.

Received August 13, 1996; revised December 12, 1996; accepted December 31, 1996